CONF-880534--14

INVITED PAPER FOR THE 15TH EPS CONFERENCE, DUBROVNIK, 16-20 MAY 1988

HIGH POWER ION CYCLOTRON RESONANCE HEATING IN JET

The JET Team[1] - presented by J Jacquinot

JET Joint Undertaking, Abingdon, Oxon, OX14 3EA, UK

CONF-880534--14

DE89 002218

ABSTRACT

Ion Cyclotron Resonance Heating (ICRH) powers of up to 17 MW have been coupled to JET limiter plasmas. The plasma stored energy has reached 7 MJ with 13 MW of RF in 5 MA discharges with $Z_{eff} \simeq 2$. When $I_p/B_\phi = 1$ MA/T the stored energy can be 50 % greater than the Goldston L mode scaling. This is due to transient stabilisation of sawteeth (up to 3 s) and to a significant energy content in the minority particles accelerated by RF (up to 30 % of the total stored energy). Central temperatures of $T_e \sim 11$ keV and $T_i \simeq 8$ keV have been reached with RF alone. (He^3)D fusion experiments have given a 60 kW fusion yield (fusion rate of 2×10^{16} s^{-1} in the form of energetic fast particles (14.7 MeV(H), 3.6 MeV(He^4)) in agreement with modelling. When transposing the same calculation to a (D)T scenario, Q is predicted to be between 0.2 and 0.8 using plasma parameters already achieved. For the first time, a peaked density profile generated by pellet injection could be reheated and sustained by ICRF for 1.2 s. Electron heat transport in the central region is reduced by a factor 2 to 3. The fusion product $n_{io}\tau_E T_{io}$ reaches 2.2×10^{20} m^{-3}.s.kev in 3 MA discharges which is a factor of 2.3 times larger than with the normal density profile.

KEYWORDS

ICRH, Tokamak, Confinement, Scaling, Fusion Yield, Heating Scenarios, Fast Ions, Pellet, Peaked Density Profiles.

INTRODUCTION

Following closely a programme established in 1982, JET has completed the installation of 8 antenna generator units in July 1987. The power plant can deliver 24 MW for 20 s in a well matched load placed at the generator output. Taking into account the losses in the transmission line, in the antenna screen and reflection, the maximum effective wave power launched in the Torus was about 15 MW for usual plasmas conditions. It reached 17 MW in some cases. This new antenna system incorporates modifications to the internal structure in order to offer a choice of $k_\parallel$ spectra found useful in previous experiments (Jacquinot, 1987a, 1987b).

Since July 1987, the ICRF system has been mainly involved in 3 topics of the JET programme:

(i) High power heating of "limiter" discharges, ie with a boundary defined by the belt limiter or by the antenna side protection. The emphasis was placed on high current (up to 6 MA). A limited number of experiments were devoted to high β targets.

(ii) High fusion yield experiments using either the fundamental cyclotron acceleration of the He^3 minority ions to an energy close to the maximum of the (D-He^3) fusion cross section (0.4 MeV) or, in combination with D beam injection, the second harmonic acceleration of D ions to maximise the D-D fusion reaction.

[1]For list of authors, see A Gibson and others, these proceedings

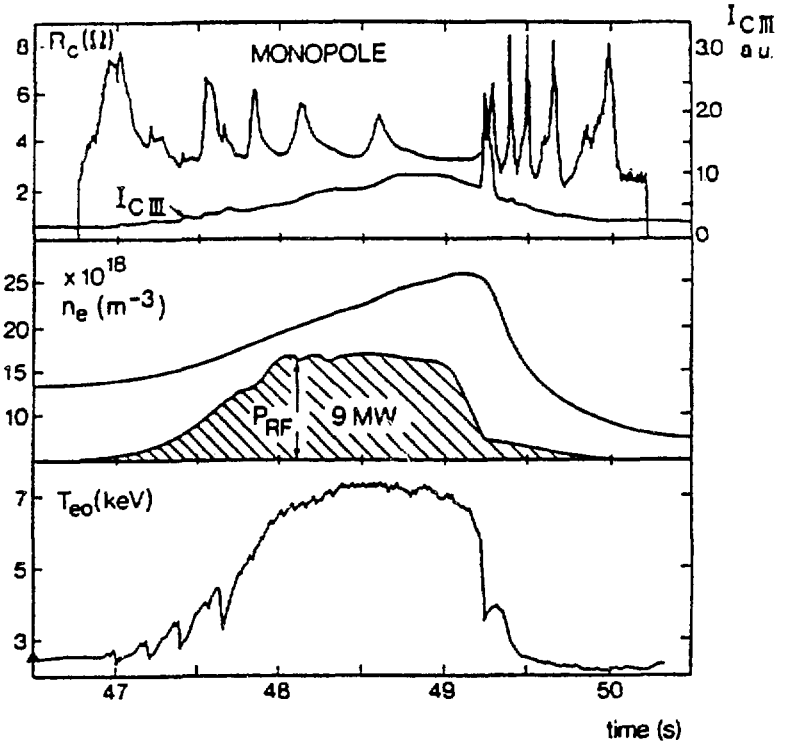

Fig. 1. Time evolution of the antenna loading resistance, intensity of CIII line radiation, volume average electron density and central electron temperature. Radial eigenmodes modify R_c but have no effect on T_{eo} and on the impurity radiation from the edge.

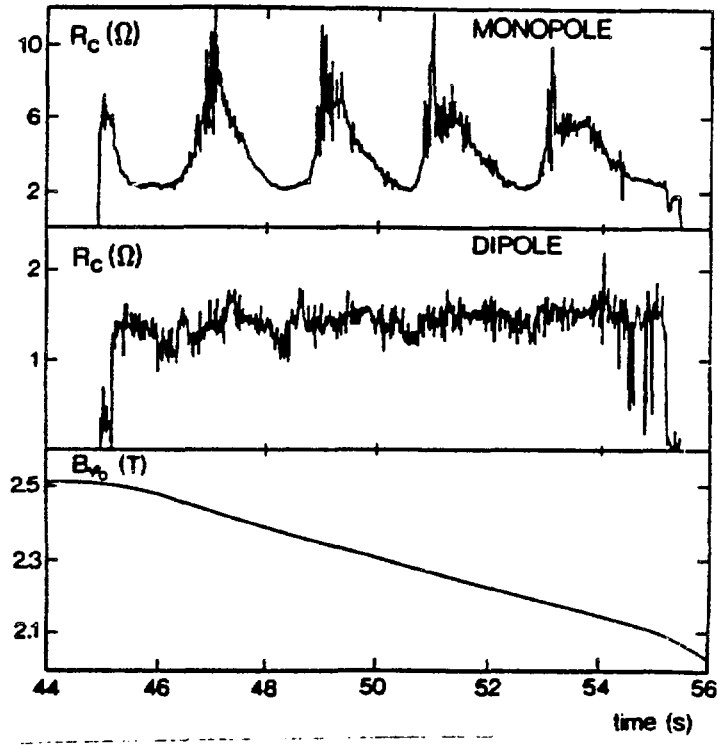

Fig. 2. Loading resistance with monopole and dipole phasing. Eigenmodes appear only for monopole phasing and are identified by their spacing during a toroidal field scan.

(iii) Heating pellet fuelled discharges with particular emphasis on a plasma target exhibiting a peaked density profile.

A very limited amount of time was devoted to coupling ICRH power into single null X point plasmas. The result was disappointing as no H-mode could be generated or sustained. Thereafter, the X point programme concentrated on using neutral beam injection.

This paper is organised as follows:

The first part describes briefly the ICRH system. The consequences of its unusual features are discussed, eg monopole versus dipole and the effect of the screen angle.

The power deposition profile and the energy stored in fast particles are discussed in a second part using power modulation during monster sawteeth to investigate the power balance with increased accuracy.

The third part examines the results of high fusion yield experiments and attempts to extrapolate the results to the most promising scenario which involves fundamental cyclotron acceleration of a large minority of deuterons in a tritium plasma.

The global performance in limiter plasmas is the subject of the next 2 parts. The emphasis is placed on the best operating regimes characterised by on axis ICRF heating producing long sawteeth and a large component of the fast ions. The recent improvement of central confinement obtained with combined operation of Pellets and ICRF are also presented.

The last part summarises the results and mentions the area of future development.

SPECIAL FEATURES

Homodyne Drive and Eigenmodes, Monopole versus Dipole, Screen Angle

The JET ICRF system has been described previously (Kaye, 1987; Wade, 1985) and it is summarised by the following table:

TABLE 1 JET ICRH System

Power	- 8 units of 3 MW (20 s) with 16 power tetrodes.
Frequency	- 23 to 57 MHz in 8 preset frequency bands.
Antennas	- 8 units, each with 2 inputs with either in phase drive (monopole) or out of phase drive (dipole). - water cooling of the screen (nickel). - screen angle: 15°. - location on the low field side between 2 belt limiters (carbon tiles).

Each unit can be driven either independently (heterodyne drive) or by a common oscillator (homodyne drive). The experiments analysed in this paper have all been obtained in the latter mode of operation which avoids problems of cross-talk and beat oscillations between adjacent frequencies. Homodyne drive imposes a phase relationship in the antenna array. All power units are driven at present with an identical input phase. However, the phase of the output of the amplifier units is not monitored. The phase control system, to be installed after June 1988, will allow to launch a partially travelling wave (directivity 20 to 25 %).

$k_{\parallel}$ Spectrum and Eigenmodes

The new antennae are equipped with central conductors having a wider toroidal extent (40 cm instead of 32 cm). This increased width and the precise phasing of the current flowing in the 2 conductors separated by a larger gap (20 instead of 10 cm) give a $k_{\parallel}$ spectrum far more accurately defined than in all previous ICRF experiments. In monopole operation, the spectrum at the antenna is centred on $k_{\parallel} = 0$ with a half width of $\pm$ 4.5 m^{-1}; in dipole operation the peak of the spectrum is at $k_{\parallel} = \pm$ 7 m^{-1} and the half width is $\pm$ 3.5 m^{-1}.

With such a narrow spectrum, the coupling resistance ($R_c = 2 Z_o^2 P/U_A^2$; Z_o characteristic impedance of the antenna, P net coupled power, U_A peak voltage of the antenna) exhibits a periodic resonance structure when either the toroidal field or the plasma density is scanned (Figs. 1 and 2). The resonance structure is more pronounced in monopole operation and when the plasma is cold. A detailed analysis (Stix, 1975) has identified the structure to be radial eigenmodes of waves reflecting back and forth between the low field side cut-off located close to the outside wall and the ion-ion hybrid cut-off normally placed close to the magnetic axis. Calculations (Colestock, 1988) taking into account the damping of the fast magnetosonic wave due to both mode conversion and direct cyclotron and electron absorption are in close agreement with the observed resonance structure.

It is important to note that these eigenmodes have no influence on the heating efficiency (Fig. 2) or on the impurity release. However they pose a technical challenge for the antenna matching system. The JET matching feedback loop based on the impedance transformation at the end of a long transmission line, produced by a small frequency change (- 50 KHz), has been effective in following these large coupling changes.

Dipole versus Monopole

Operation with the dipole phasing when compared to the monopole phasing is characterised by the following aspects:

(a) The coupling resistance is lower (Fig. 2) and decreases faster with plasma-antenna distance.

(b) The radiated power and the nickel contamination is lower.

(c) The power threshold for the monster sawtooth is higher.

Point (b) is particularly relevant to the experiments with powers exceeding 15 MW as the amount of nickel released from the antenna screen may cause disruptions. In hydrogen minority heating, the nickel concentration is approximately of factor 2 lower in dipole operation. In helium 3 minority schemes, the reduction is more pronounced and a decrease by a factor of 4 has been observed.

Since the calculated damping per pass is larger in dipole phasing and with H minority heating one is tempted to suggest that edge absorption enhanced by multiple reflections is responsible for the impurity release. This explanation is contradicted, however, by the observation that we have not found any correlation of the nickel and carbon release with the eigenmode structure which is a direct measure of multiple reflections. The experiments with reverse toroidal field (see below) suggest instead that direct slow wave coupling by the antenna is responsible for the edge effects induced by ICRF.

Screen Angle

The screen elements of the antenna screens are inclined by an angle of 15° with respect to the horizontal plane. The elements are designed to be aligned with the Tokamak magnetic field in full bore 5 MA discharges. This design was chosen to optimise coupling to the fast magnetosonic wave and to minimise the excitation of slow waves which require a finite value of $E_\parallel$, the wave electric field parallel to the static magnetic field.

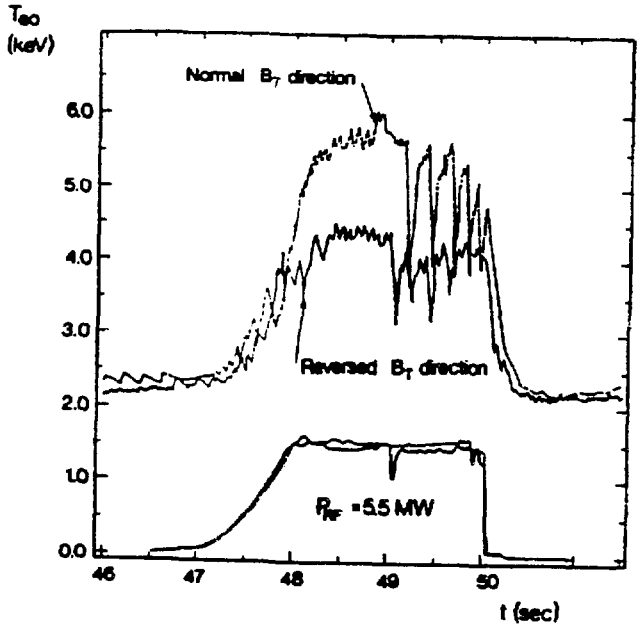

Fig. 3. Evolution of the central electron temperature T_{eo} for 2 values of the angle θ_A between the screen bars and the local magnetic field: θ_A = 5° for the "normal" case and 20° for the "reverse" case.

A series of experiments (Bures, 1988) have been performed with 2 MA discharges (H minority, 2.1 T) differing only by the direction of the static toroidal magnetic field. With the "normal" direction, the angle between the field and the elements was 5°, with the reverse direction, the angle became 25°. The overall heating characteristics are far better in the "normal" case. In particular:

(a) The heating efficiency (ΔT_e, ΔW) is 30 % higher. Figure 3 illustrates the difference in evolution of T_{eo}. Both discharges switch to a monster sawtooth, but the duration is longer with the normal field direction.

(b) The release of nickel, carbon, oxygen during the heating is about a factor of 3 (Ni) and 2 for (C and O) lower in the normal case. The total radiated power is 40 % of the input power in the reverse case compared to 30 % in the normal configuration.

(c) R_c is lower in the reverse field case (typically 4.5 ohms in the "normal", 3 ohms in the reverse case). The eigenmode structure is less apparent in the reverse case.

(d) The perturbation of the scrape off layer is lower in the normal case (less flattening of the density and temperature profile).

These results suggest that an ICRF antenna can couple a considerable amount of slow wave if the screen elements have an angle with the static magnetic field. This slow wave does not contribute to bulk heating and may generate impurity release by edge interaction. It is likely that, even in the normal case, a significant amount of slow wave power is being coupled and is responsible for some deleterious edge effects. This intepretation is also compatible with the insensitivity of impurity release by the eigenmodes of the fast wave.

DEPOSITION PROFILE, ENERGY STORED IN THE FAST MINORITY IONS

In some conditions, called "Monster Sawteeth" the plasma is very quiescent during a period of up to 3 s. Modulation of the ICRF power during this period gives accurate insight in the energy balance and in the power deposition profile (Tibone, 1988). So far, results have only been obtained in the He^3 and H minority case with monopole phasing.

The response to this modulation of the diamagnetic loop (W_{dia}) and MHD signals (W_{MHD}) shows that about 75 ± 10 % of the input power appears in the total stored energy (presumably the rest is deposited in outer layers and is not measured due to finite time response of the diagnostics). The same measurements used to derive the quantity $4(W_{dia} - W_{MHD})/3$ show that most of the RF power (up to 70 %) first appears in the form of plasma energy with strong perpendicular anisotropic tail which subsequently relaxes on the electrons.

Direct electron heating is apparent in the He^3 minority case with an instantaneous response of local ECE measurements at the onset of each step of the square wave modulation. Direct electron heating amounts to about 5 to 10 % in the H minority case and 10 to 30 % in He^3 minority heating case.

The power deposition profile appears highly localised in the vicinity of the minority cyclotron resonance as already mentioned in a previous paper (Jacquinot, 1987). It is well described by a gaussian profile with a 20 cm e-folding length in agreement with full wave or ray-tracing calculations (Tibone, 1988).

In the quasi-stationary state, the plasma contains a significant amount of energy stored in fast ions (W_f). Figure 4 compares $W_{f\ exp}$ to a calculated

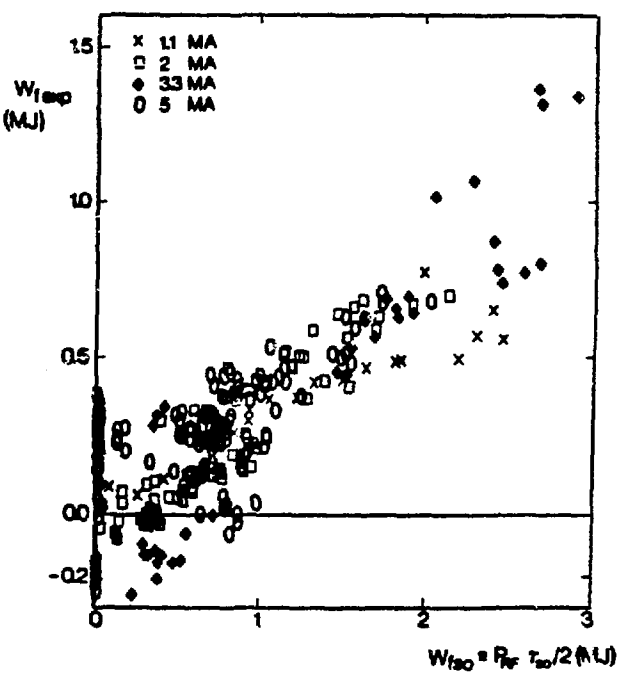

Fig. 4. Energy stored in fast particles (fundamental resonance of minority species) versus $P_{RF}\ \tau_{So}/2$ where τ_{So} is the classical Spitzer slowing down time calculated for the parameters of the plasma centre.

value W_{fso} based on Stix's quasi linear treatment (Stix, 1975) of an energetic minority tail. $W_{f\ exp}$ is deduced from the difference between the diamagnetic energy and a thermal kinetic energy (volume integration of $n_eT_e + n_iT_i$). The offset in Fig. 4 is due to systematic errors. W_{fso} is equal to:

$$W_{fso} = P_{RF} < \tau_{so} > /2$$

where P_{RF} is the coupled power and $< \tau_{so} >$ is the classical Spitzer slowing down time by electron drag using the central value of n_e and T_e (from the ECE system). A good agreement is found between the scaling of the 2 quantities. The calculated value is a factor 2 too high. The difference results from the use in the calculation of central values of n_e and T_e. A full calculation (Eriksson, 1988) including profiles effects is in close agreement with the observation.

W_f amounts typically to 15 % of the stored energy in usual belt limiter discharges. It can reach 30 % (about 2 MJ) for the lowest density plasmas using a double null X point configuration. The entire data base for W_f scales, as expected, with $T_e^{3/2}/n_e$ suggesting that the fast particles have a classical slowing down time.

(He^3)-D AND (D)-T HIGH FUSION YIELD SCENARIOS

The fundamental cyclotron acceleration of He^3 minority ions gives the opportunity to study experimentally non thermal high fusion yield schemes and to simulate (D)T scenarios where deuterium would replace helium 3. The basic reactions are:

$$D + He^3 \rightarrow H(14.7\ MeV) + He^4(3.6\ MeV)$$
$$D + He^3 \rightarrow L_i^5 + \gamma(16.6\ MeV)$$

The second reaction occurs with a much smaller probability via the same resonance; it was used as a diagnostic (measurement of the 16 Mev γ production (Sadler, 1988)) to monitor the fusion yield.

Figure 5 summarises the experimental results (Cottrell, 1988). With 11.5 MW of ICRF in 3 MA plasmas, about 60 kW of fusion power has been generated in charged particles corresponding to

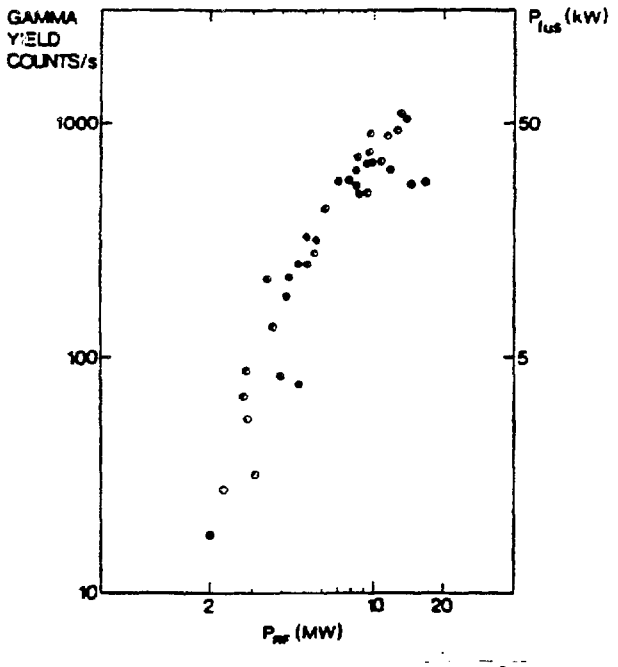

Fig. 5. Fusion power from D-He^3 reactions versus coupled RF power. He^3 minority heating in a deuterium plasma.

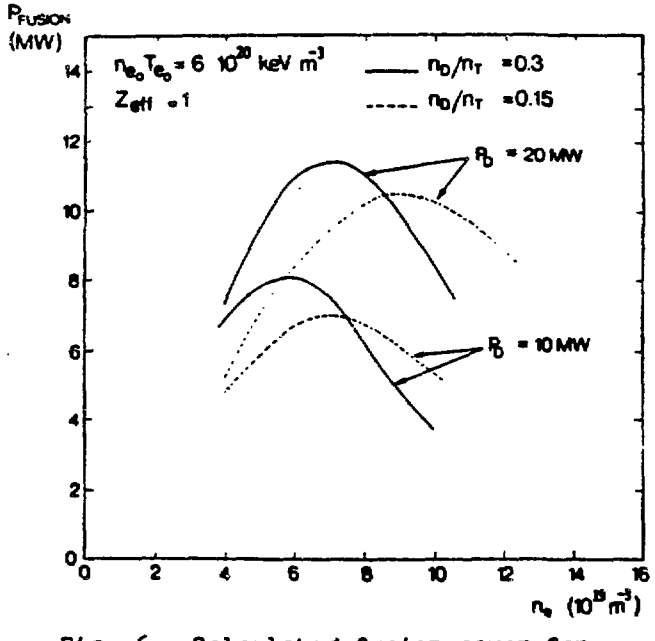

Fig. 6. Calculated fusion power for D minority heating in a tritium plasma. The calculation takes into account the profiles of the power deposition and of the plasma parameters. P_D is the RF power coupled to deuterons (- 85 % of the coupled RF power).

an effective Q - 0.5 % and a fusion reaction rate of 2 x 10^{14} s^{-1}. This value is by a factor 3 less than the calculated optimum which is reached when the energy of the minority corresponds to the maximum of the fusion cross section. The measured fusion yield agrees well with simulations based on Fokker-Plank calculations and measured plasma parameters (Eriksson, 1988).

Carrying over these encouraging results to a (D)-T plasma requires a number of adjustments:

(a) The minority concentration n_D/n_T should be increased to about 30 % and the electron density should be raised to about 6 10^{19} m^{-3}. Both measures avoid that the energy of the minority exceeds the optimum of the fusion D-T cross section.

(b) The parameters quoted in (a) necessitates using a dipole phasing ($k_{\parallel}$ = 7 m^{-1}) in order to prevent mode conversion at the D-T hybrid resonance resulting in direct electron damping. TTMP and electron Landau interactions with the fast magnetosonic wave is estimated to damp - 15 % of the coupled wave power into electrons if T_{eo} = 10 keV.

(c) The damping per pass is expected to be large (90 % per pass). Interaction with the second harmonic resonance of tritium on the extreme low field side is prevented by locating the resonance either on axis or slightly shifted to the low field side.

Figure 6 gives the enhancement of fusion reactivity expected from the deuterium tail as a function of P_d, the RF power coupled to the deuterons. This calculation is a Fokker Planck treatment taking into account (Eriksson, 1988) the profiles of the power deposition and of the plasma parameters. The product n_{eo} T_{eo} has been fixed to 6 10^{20} (m^{-3} keV), a value achieved with 10 MW of ICRF being the only additional heating source. Q ≥ 0.5 can be achieved if Z_{eff} can be maintained close to unity. A self consistent set of parameters necessary to achieve Q = 1 is given in Table 2.

TABLE 2 Conditions for Q = 1 required in a (D)T Plasma with ICRH alone

Power to D tail:	≥ 20 MW
n_{eo}	: ≈ 7 10^{19} m^{-3}
n_D/n_T	: ≈ 0.2
τ_E	: ≥ 0.6 s
Z_{eff}	: ≤ 2

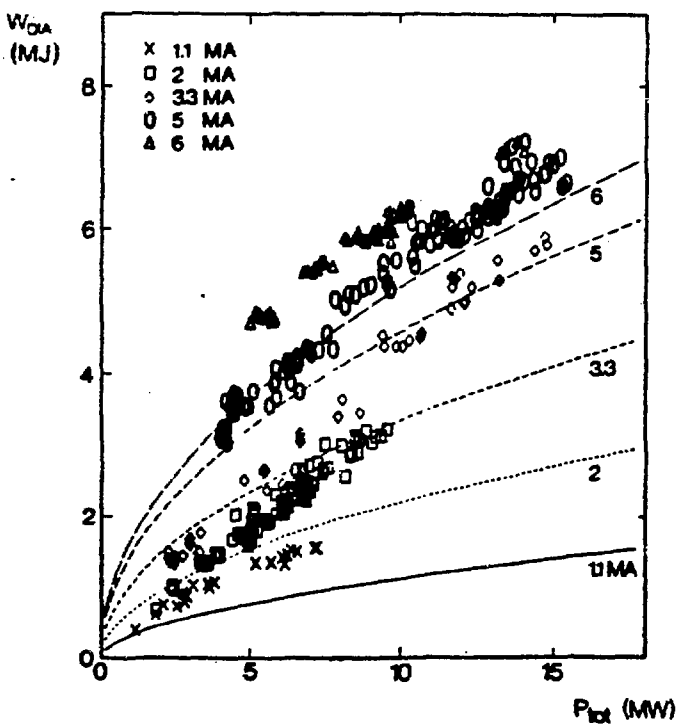

Fig. 7a. Stored energy (diamagnetic measurements) versus input power for H minority heating and comparison to the Goldston scaling.

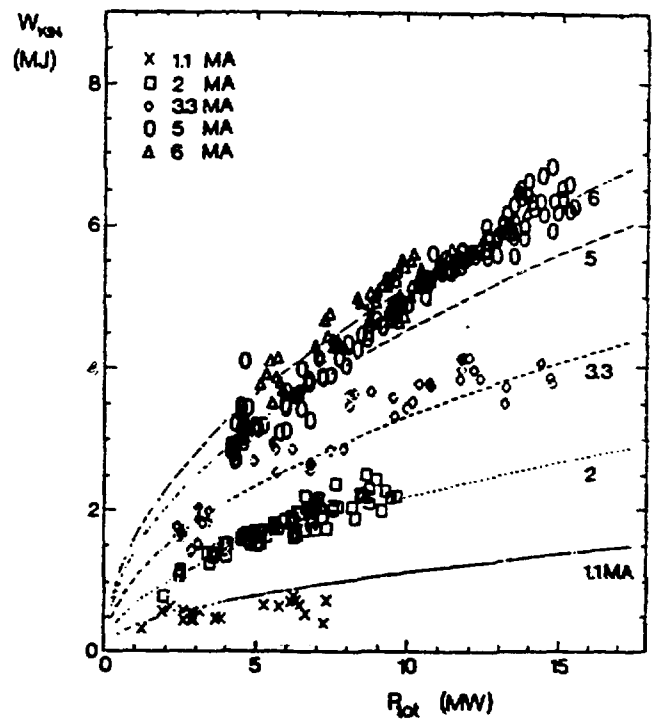

Fig. 7b. Kinetic stored energy (volume integration of $n_eT_e + n_iT_i$) for the same data set as Fig. 7a.

LIMITER PLASMAS, GLOBAL CONFINEMENT AND I_p SCALING

A new result obtained by ICRF heating of limiter plasmas is the attainment of regimes in which the total stored energy can be up to a factor 1.5 greater than predicted by the Goldston L mode scaling (Goldston, 1984) (Fig. 7a).

Contrary to the H-mode, there is little improvement in the kinetic energy content (Fig. 7b) and most of the improvement comes from the storage of fast particles and from the development of a stable peaked temperature profile. Table 3 summarises the conditions for obtaining this regime. The narrow power deposition of ICRF and its stabilising effect on the sawteeth play a major role.

TABLE 3 Conditions for Improved Stored Energy in Limiter Plasmas

Peaked deposition profile:	on axis ICRF heating (all minority scenarios)
Long sawteeth	: $\tau_{ST} \geq \tau_E$, ie monsters
Moderate densities	: $n_e \leq 4\ 10^{19}$ cm^{-3}; large W_f, ie $W_f/W \geq 0.15$
I_p/B_ϕ	: $\simeq$ 1 MA/T, eg $q_{cyl} = 3.3$

In the best conditions, the incremental confinement time, τ_{inc}, reaches 340 ms in 3.3 MA, 2.8 T plasmas (Fig. 7c). τ_{inc} first increases with I_p, reaching an optimum (Bhatnagar, 1988) for I/B = 1 MA/T then decreases to $\simeq$ 220 ms in 6 MA plasmas. This behaviour is correlated with the period of the sawteeth which also reaches a maximum ("monster" of up to 3 s) when I/B ~ 1 MA/T.

At low or medium I_p values, no difference in stored energy is found between the 4 ICRF scenarios (H, He^3, monopole, dipole). At 5 MA with He^3 minority heating, large fishbone-like activities develop early in the sawtooth period and prevent the rise of T_e. Then τ_{inc} is

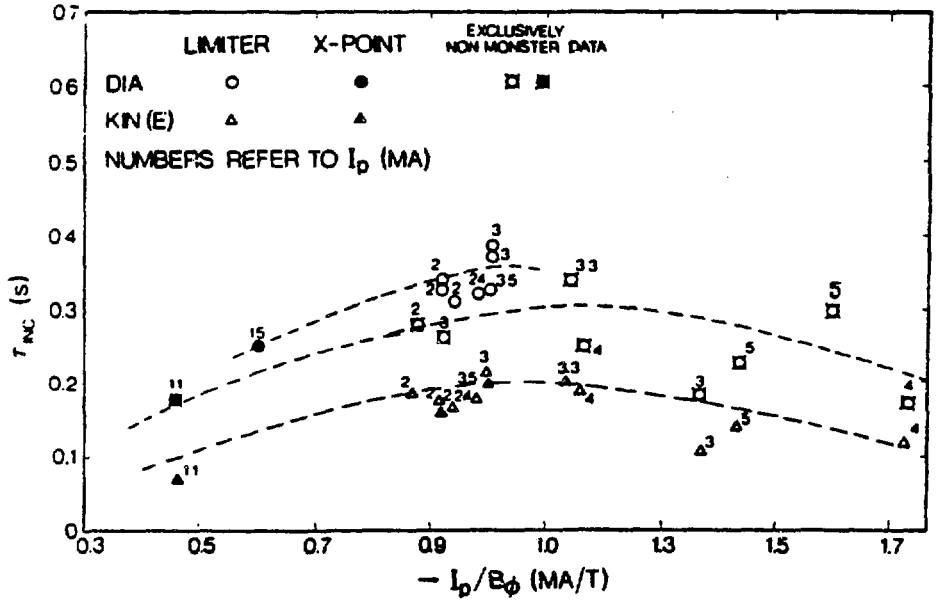

Fig. 7c. Incremental confinement time of the stored energy (diamagnetic; DIA) and the electron thermal energy content (KIN(E)) versus I_p/B_ϕ

only 250 ms in this regime. It is not clear why this phenomenon does not appear in the H minority case in 5 MA plasmas. In this case τ_{inc} is improved (300 ms) and 7 MJ has been obtained with a total input power of 15 MW.

In the series of experiments of Fig. 7a, the total radiated power was about 40 % of the input power. Since the radiated power is peaked at the plasma edge, it plays no role in the energy balance in the plasma core. Z_{eff} was about 2 in high current discharges and $\geq$ 3 below 3 MA.

The central electron and ion temperatures are presented in Figs. 8 and 9. Whilst T_{eo} follow a linear scaling with $P_{tot}/\langle n_e \rangle$, the ion temperature tends to saturate showing that the hydrogen minority becomes decoupled from the plasma ions at high power density. Higher ion temperatures (up to 8 keV) have been obtained either with He^3 minority heating (Start, 1988) at high He^3 concentration (11 %) and using dipole phasing or during the heating of a peaked

density profile produced by pellets in 3 MA plasmas. In the latter case, T_{eo} (ECE) = 11 keV, T_{io} = 7.8 keV, with P_{RF} = 7.4 MW. The $n_{io}\tau_E T_{io}$ values obtained with ICRF in limiter plasmas are summarised in Fig. 10.

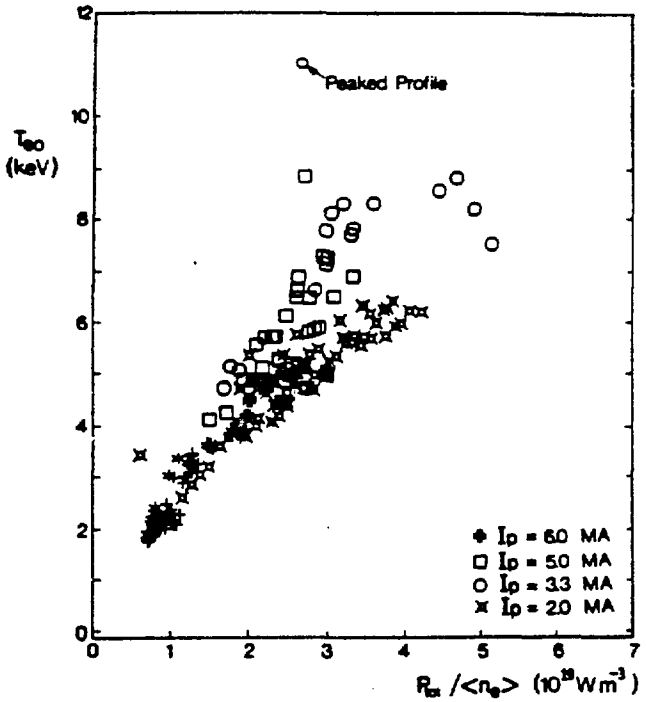

Fig. 8. Central electron temperature versus $P_{tot}/< n_e >$. The case denominated "peaked profile" was created by pellet injection.

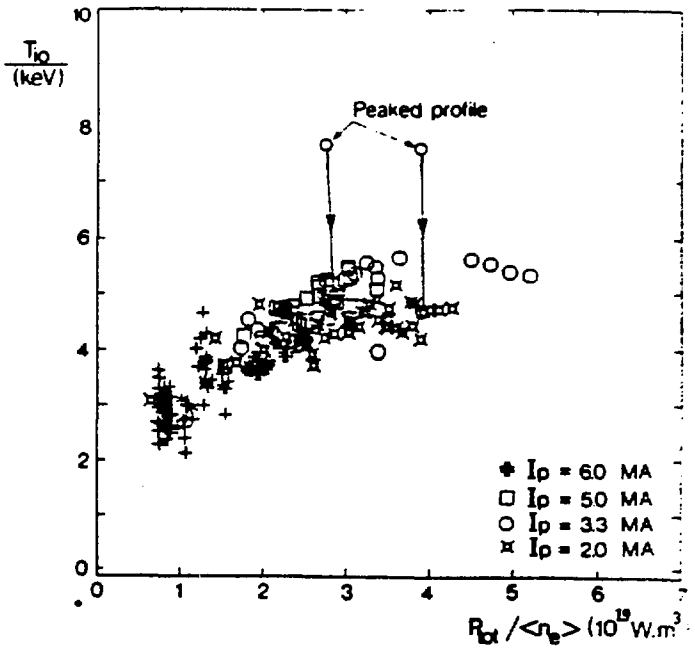

Fig. 9. Central ion temperature versus $P_{tot}/< n_e >$. T_{io} is deduced from Doppler broadening of a Ni line.

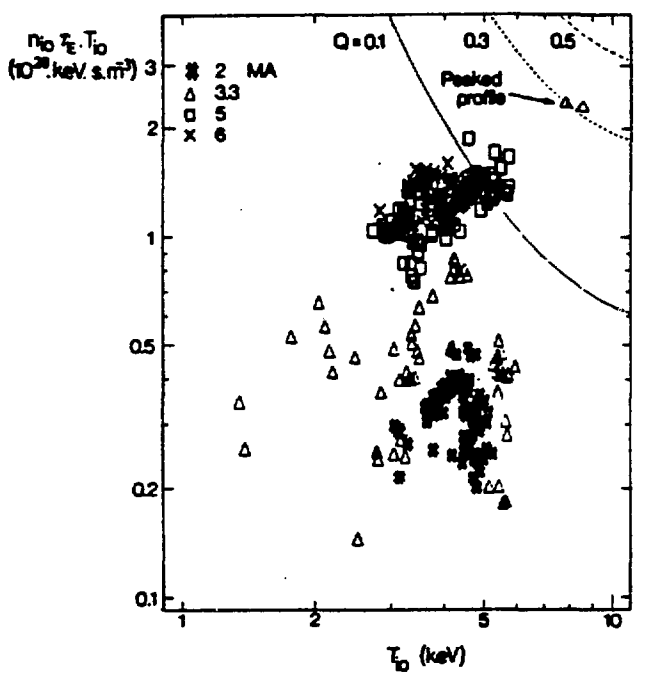

Fig. 10. Fusion parameter, $n_{io}\tau_E T_{io}$ versus the central ion temperature T_{io}.

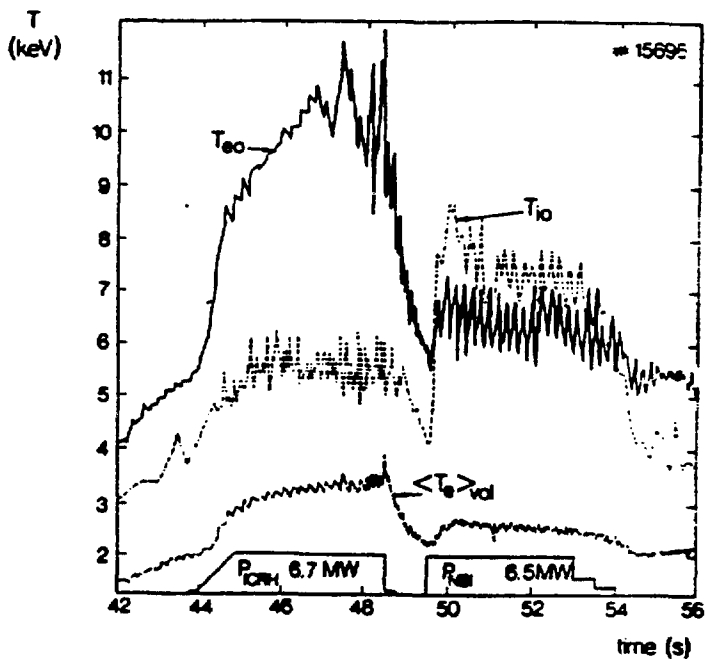

Fig. 11. Evolution of the central electron and ion temperature for ICRH or NBI during the same discharge (3 MA, 3.1 T, H minority in a helium plasma).

It is instructive to compare ICRF to neutral beam (NBI) heating in the same pulse with the same power in the conditions corresponding to the improved L mode scaling (3 MA, 3.15 T, H minority, dipole).

The behaviour of the ion and electron temperature is remarkably different (Fig. 11). With NBI, one always obtains $T_i > T_e$ while ICRF always yields $T_e > T_i$. Figure 12 shows that the radiated power with ICRF is generally larger than with NBI despite a somewhat lower density (~ 10 %) in the ICRF case. However the stored energy is significantly higher with ICRF probably as a result of a more peaked deposition profile and longer sawtooth periods.

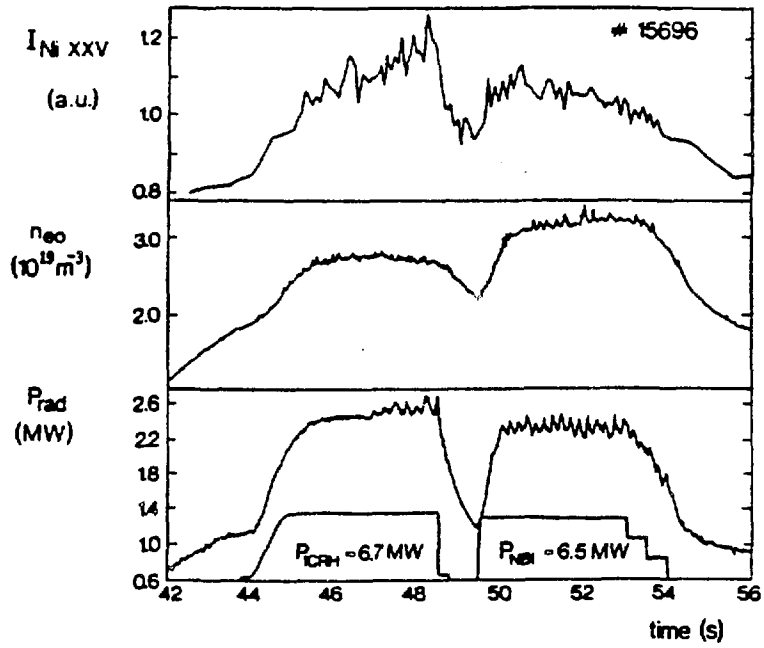

Fig. 12. Evolution of nickel contamination, central density and total radiated power for ICRH and NBI during the same discharge (same case as Fig. 11).

HEATING PEAKED DENSITY PROFILES

It has been suggested (Furth, 1986; Schmidt, 1987) that central heating of a peaked density profile generated by pellet injection (Kupschus, 1988) could lead to improved energy confinement as observed in TFTR supershots.

Recent experiments have demonstrated that this improvement indeed occurs. Figures 13a and 13b show that:

(a) A reheated peaked profile can be sustained for about 1.2 s in a 3 MA discharge with pellet injection at the end of the current rise. However, the peaked profile is subject to a sudden instability (cf Fig. 13a at 44.4 s) which relaxes the profile to the usual shape (a monser sawtooth Te profile).

(b) The central energy confinement in the peaked region is improved. For 8 MW of ICRF, T_{eo} rose to 11 keV (Fig. 13b) and T_{io} to 8 keV. The T_e profile steepens showing a decrease of the electron energy transport coefficient in the centre by a factor 2 to 3 compared to the relaxed state. The fusion product $n_{io}\tau_E T_{io}$ reaches 2.2 10^{20} m^{-3} s^{-1} keV, a value 2.3 times greater than in the normal limiter discharges.

CONCLUSIONS

High power ICRF heating with up to 17 MW has been particularly successful in heating plasmas resting on toroidal belt limiters. With RF heating alone central temperatures of T_e = 11 keV and T_i = 8 keV have been reached. H minority heating and moderate plasma current give the highest incremental confinement time (τ_{inc} = 340 ms). In these discharges monster sawteeth of up to 3 s have been obtained.

Peaked profiles created by pellet injection have been reheated by ICRF. In most cases the peaked profile disappeared in 0.5 s. During the peaked density phase, the energy confinement

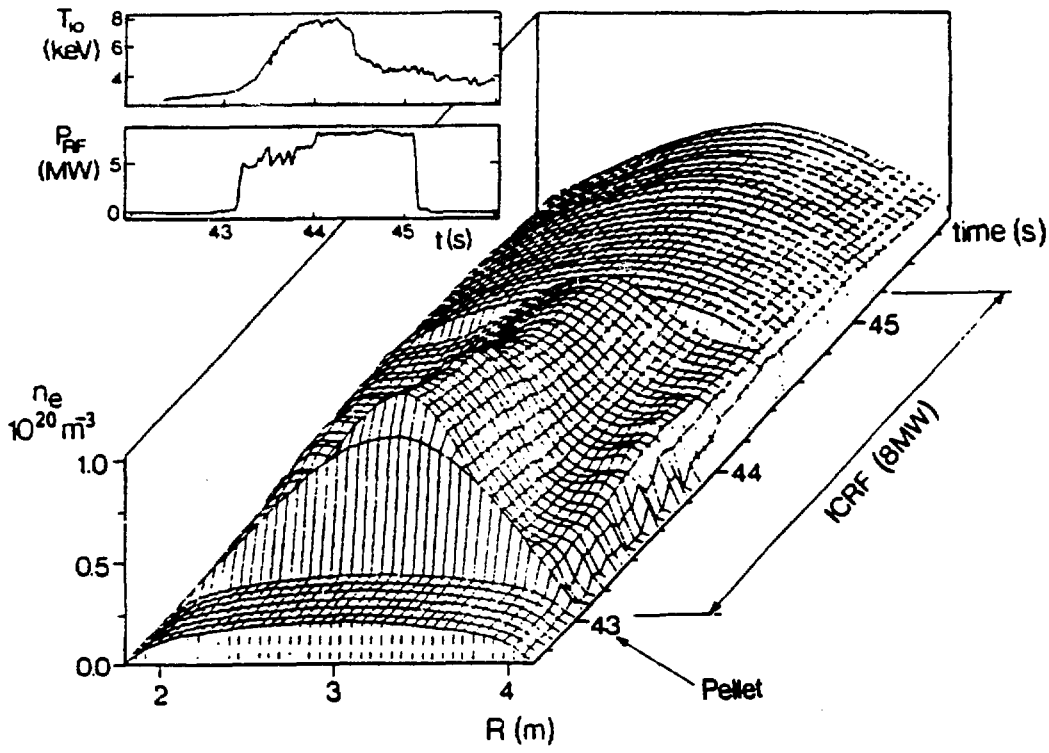

Fig. 13a. Evolution of the density profile. A peaked profile is created by a 4 mm pellet at 43 s. ICRF power is ramped up from 43.2 to 44 s and maintained constant at 8 MW until 45.2 s. Note the sudden relaxation of the profile at 44.5 s.

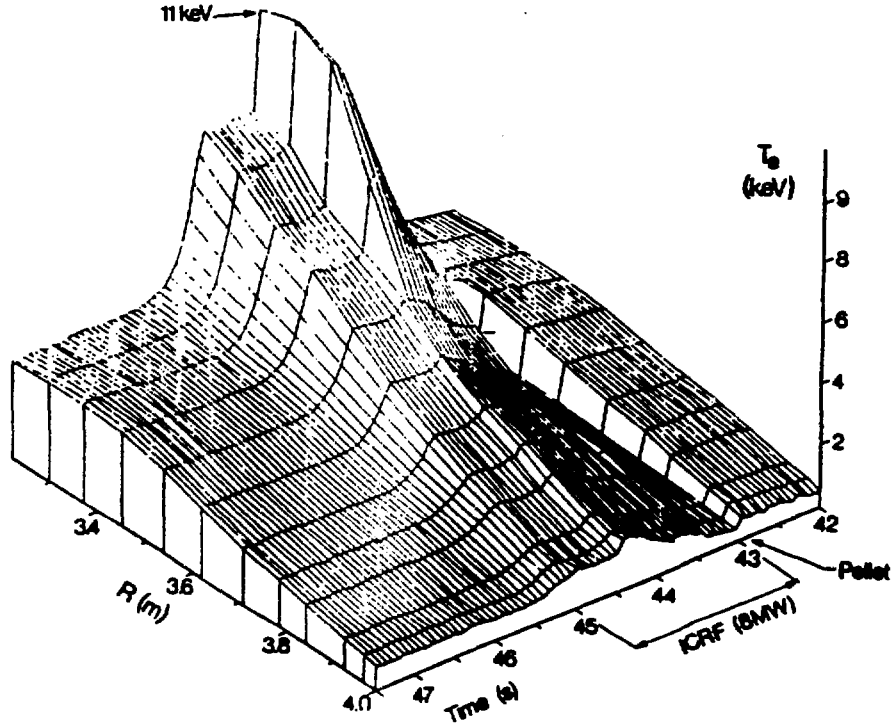

Fig. 13b. Evolution of the electron temperature profile. Note that the peaked T_e profile relaxes also at 44.5 s. The time axis has been reversed in order to show the shape of the T_e profile more clearly.

in the plasma centre ($r/a \leq 0.4$) is improved and a fusion product of $n_{io}\tau_E T_{io} = 2.2\ 10^{20}\ m^{-3}\ s\ keV$, the highest value in JET limiter discharges is obtained.

Impurities are reduced when the elements of the antenna screen are parallel to the magnetic field and when the dipole configuration is used. High power ICRF heating have been performed in 5 MA plasmas with $Z_{eff} \sim 2$.

The heating and impurity release is unaffected by the eigenmodes of the fast waves. These observations suggest that, despite the filtering effect of the screen the antenna launches some slow wave component responsible for the impurity production.

RF driven high fusion yield scenarios have been tested using the fundamental cyclotron absorption of He^3 minority ions. A maximum yield of 60 kW has been obtained in the form of charged particles. The same discharge transposed to (D)T with D minority heating would give $Q = 0.2$. Transposition of the best peaked profile heating achieved today would give $Q = 0.8$ assuming $Z_{eff} = 1$.

The JET ICRF system will be modified to allow for phasing the 8 antennae. A travelling wave with an expected maximum directivity of 20 - 25 % is expected to modify significantly the gradient of the safety factor in the central region. Screens with bars made of Beryllium will replace the present Nickel in an attempt to remove the radiation problem in the H-mode plasmas and to improve the density control by avoiding carbonised structures.

ACKNOWLEDGEMENT

Pellet injection results were obtained under a collaboration agreement between the JET Joint Undertaking and the US Department of Energy.

REFERENCES

Bhatnagar, V. P. and others (1988). This conference.
Bures, M. and others(1988). This conference.
Colestock, P. (1988). Private communication.
Cottrell, G. A. and others. This conference.
Eriksson, L. G. and T. Hellsten (1988). Private communication.
Furth, H. P. (1986). Plasma Phys. Control Fusion 28, 1305.
Goldston, R. J. (1984). Plasma Phys. Control Fusion 26, 87.
Jacquinot, J. and JET Team (1987). Proc. 11th Int. Conf., Kyoto (1986), Vol. 1, IAEA, Vienna, 449.
Jacquinot, J. and others (1987). Proc. 7th Top. Conf. on Applications of Radio Frequency Power to Plasmas, Kissimee. AIP Conf. Proc. 159, 220.
Kaye, A. S., J. Jacquinot, P. Lallia and T. Wade (1987). Fusion Technology, Vol. 2, 203.
Kupschus, P. and others (1988). This conference.
McCarthy, A. L. and others (1988). This conference.
Sadler, G. and others (1988). This conference.
Schmidt, G. and others (1987). Proc. 11th Int. Conf., Kyoto 1986, Vol. 1, IAEA, Vienna 171.
Start, D. and others (1988). This conference.
Stix, T. H. (1975). Nuclear Fusion, 15, 737.
Tibone, F., M. P. Evrard and others (1988). This conference.
Wade, T. (1985). Proc. 11th Symp. Fusion Engineering, Austin, Texas.

APPENDIX.1

THE JET TEAM

JET Joint Undertaking, Abingdon, Oxon, OX14 3EA, U.K.

J.M.Adams[1], F.Alladio[4], H.Altmann, R.J.Anderson, G.Appruzzese, W.Bailey, B.Balet, D.V.Bartlett, [redacted][24], K.Behringer, A.C.Bell, P.Bertoldi, E.Bertolini, V.Bhatnagar, R.J.Bickerton, A.Boileau[3], T.Bonicelli, S.J.Booth, G.Bosia, M.Botman, D.Boyd[31], H.Brelen, H.Brinkschulte, M.Brusati, T.Budd, M.Bures, T.Businaro[4], H.Buttgereit, D.Cacaut, C.Caldwell-Nichols, D.J.Campbell, P.Card, J.Carwardine, G.Celentano, P.Chabert[27], C.D.Challis, A.Cheetham, J.Christiansen, C.Christodoulopoulos, P.Chuilon, R.Claesen, S.Clement[30], J.P.Coad, P.Colestock[6], S.Conroy[13], M.Cooke, S.Cooper, J.G.Cordey, W.Core, S.Corti, A.E.Costley, G.Cottrell, M.Cox[7], P.Cripwell[13], F.Crisanti[4], D.Cross, H.de Blank[16], J.de Haas[16], L.de Kock, E.Deksnis, G.B.Denne, G.Deschamps, G.Devillars, K.J.Dietz, J.Dobbing, S.E.Dorling, P.G.Doyle, D.F.Düchs, H.Duquenoy, A.Edwards, J.Ehrenberg[14], T.Elevant[12], W.Engelhardt, S.K.Erents[7], L.G.Eriksonn[5], M.Evrard[2], H.Falter, D.Flory, M.Forrest[7], C.Froger, K.Fullard, M.Gadeberg, A.Galetsas, R.Galvao[4], A.Gibson, R.D.Gill, A.Gondhalekar, C.Gordon, G.Gorini, C.Gormezano, N.A.Gottardi, C.Gowers, B.J.Green, F.S.Griph, M.Gryzinski[26], R.Haange, G.Hammett[6], W.Han[9], C.J.Hancock, P.J.Harbour, N.C.Hawkes[7], P.Haynes[7], T.Hellsten, J.L.Hemmerich, R.Hemsworth, R.F.Herzog, K.Hirsch[14], J.Hoekzema, [redacted][16], J.How, M.Huart, A.Hubbard, T.P.Hughes[32], M.Hugon, M.Huguet, J.Jacquinot, O.N.Jarvis, [redacted]J.C.Jennigan[24], E.Joffrin, E.M.Jones, L.P.D.F.Jones, T.T.C.Jones, J.Källne, A.Kaye, B.E.Keen, M.Keilhacker, G.J.Kelly, A.Khare[15], S.Knowlton, A.Konstantellos, M.Kovanen[21], P.Kupschus, P.Lallia, J.R.Last, L.Lauro-Taroni, M.Laux[33], K.Lawson[7], E.Lazzaro, M.Lennholm, X.Litaudon, P.Lomas, M.Lorentz-Gottardi[2], C.Lowry, G.Magyar, D.Maisonnier, M.Malacarne, V.Marchese, P.Massmann, L.McCarthy[28], G.McCracken[7], P.Mendonca, P.Meriguet, P.Micozzi[4], S.F.Mills, P.Millward, [redacted][24], A.Moissonnier, P.L.Mondino, D.Moreau[17], P.Morgan, H.Morsi[14], G.Murphy, M.F.Nave, M.Newman, L.Nickesson, P Nielsen, P.Noll, W.Obert, D.O'Brien, J.O'Rourke, M.G.Pacco-Düchs, M.Pain, S.Papastergiou, D.Pasini[20], M.Paume[27], N.Peacock[7], D.Pearson[13], F.Pegoraro, M.Pick, S.Pitcher[7], J.Plancoulaine, J-P.Poffé, F.Porcelli, R.Prentice, T.Raimondi, J.Ramette[17], J.M.Rax[27], C.Raymond, P-H.Rebut, J.Removille, F.Rimini, D.Robinson[7], A.Rolfe, R.T.Ross, L.Rossi, G.Rupprecht[14], R.Rushton, P.Rutter, H.C.Sack, G.Sadler, N.Salmon[13], H.Salzmann[14], A.Santagiustina, D.Schissel[25], P.H.Schild, M.Schmid, G.Schmidt[6], R.L.Shaw, A.Sibley, R.Simonini, J.Sips[16], P.Smeulders, J.Snipes, S.Sommers, L.Sonnerup, K.Sonnenberg, M.Stamp, P.Stangeby[19], D.Start, C.A.Steed, D.Stork, P.E.Stott, T.E.Stringer, D.Stubberfield, T.Sugie[18], D.Summers, H.Summers[30], J.Taboda-Duarte[22], J.Tagle[30], H.Tamnen, A.Tanga, A.Taroni, C.Tebaldi[23], A.Tesini, P.R.Thomas, E.Thompson, K.Thomsen, P.Trevalion, M.Tschudin, B.Tubbing, K.Uchino[29], E.Usselmann, H.van der Beken, M.von Hellermann, T.Wade, C.Walker, B.A.Wallander, M.Walravens, K.Walter, D.Ward, M.L.Watkins, J.Wesson, D.H.Wheeler, J.Wilks, U.Willen[12], D.Wilson, T.Winkel, C.Woodward, M.Wykes, I.D.Young, L.Zannelli, M.Zarnstorff[6], D.Zasche[14], J.W.Zwart.

PERMANENT ADDRESS

1. UKAEA, Harwell, Oxon UK
2. EUR-EB Association, LPP-ERM/KMS, B-1040 Brussels, Belgium.
3. Institute National de Recherches Scientifiques, Quebec, Canada.
4. ENEA-CENTRO Di Frascati, I-00044 Frascati, Roma, Italy
5. Chalmers University of Technology, Goteborg, Sweden
6. Princeton Plasma Physics Laboratory, New Jersey, USA
7. UKAEA Culham Laboratory, Abingdon, Oxon. UK
8. Plasma Physics Laboratory, Space Research Institute, São José dos Campos, Brazil
9. Institute of Mathematics, University of Oxford, UK.
10. CRPP/EPFL, 21 Avenue des Bains, CH-1007 Lausanne, Switzerland.
11. Swedish Energy Research Commission, S-10072 Stockholm, Sweden.
12. Imperial College of Science and Technology, University of London, UK
13. Max Planck Institut fur Plasmaphysik, D-8046 Garching bei Munchen, FRG.
14. Institute for Plasma Research, Gandhinagar Bhat Gujat, India.
15. FOM Instituut voor Plasmafysica, 3430 BE Nieuwegein, The Netherlands
16. Commissariat à l'Energie Atomique, Cadarache, France
17. JAERI, Tokai Research Establishment, Tokai-Mura, Naka-Gun, Japan.
18. Institute for Aerospace Studies, University of Toronto, Downsview, Ontario, Canada.
19. University of Strathclyde, Glasgow, G4 ONG, U.K
20. Nuclear Engineering Laboratory, Lapeenranta University, Finland.
21. JNICT, Lisboa, Portugal.
22. Department of Mathematics, University of Bologna, Italy.
23. Oak Ridge National Laboratory, Oak Ridge, Tenn., USA
24. G.A. Technologies, San Diego, California, USA
25. Institute for Nuclear Studies, Swierk, Poland.
26. Commissariat à l'Energie Atomique, Cadarache, France
27. School of Physical Sciences, Flinders University of South Australia, South Australia 5042.
28. Kyushi University, Kasagu Fukuoka, Japan.
29. Centro de Investigaciones Energeticas Mediombientales y Tecnologicas, Spain.
30. University of Maryland, College Park, Maryland, USA
31. University of Essex, Colchester, UK
32. Akademie der Wissenschaften, Berlin, DDR

CR 88 48 1A

DISCLAIMER